Qualitative Aspects of Neutron-Nuclear Interactions and the Optical Model*

VICTOR FRANCO†
Laboratory for Nuclear Science and Department of Physics, Massachusetts Institute of Technology, Cambridge, Massachusetts
(Received 21 July 1965)

The appearance of broad maxima and minima in the energy dependence of neutron-nuclear total and scattering cross sections below 100 MeV is given a simple explanation. Within the framework of the Glauber diffraction approximation, the general conditions for the occurrence of these maxima and minima are obtained in terms of an integral, over impact parameters, involving a phase-shift function. A modification of the approximation is employed so that the formalism may be applied below 100 MeV. The assumption that the average phase difference between that portion of the neutron wave which traverses the nucleus and that which does not is equal to an integral multiple of π at cross-section maxima and minima is shown to be incorrect. The approximations are illustrated with some optical-model calculations which indicate that the positions of the maxima and minima shift to higher energies with increasing target mass number. Some numerical calculations using the Schrödinger equation with square-well and Woods-Saxon potentials are compared with cross sections calculated from the approximation. Near the maxima, appreciable contributions come from a number of partial cross sections. The appearance of these maxima implies neither a resonance in any single partial wave nor a maximum in any single partial cross section. A brief consideration of the energy dependence in the total, absorption, and scattering cross sections separately, reveals that the principal qualitative features of the total cross section are manifest in the scattering cross section.

I. INTRODUCTION

IN 1921 Ramsauer[1] investigated the energy dependence of the cross section for low-velocity electrons scattered by argon atoms and discovered a rather surprising result. As the incident energy of the electron was increased from very small values, the cross section decreased to a relative minimum near one electron volt. As the energy was increased further, the cross section increased until it reached a relative maximum, after which it decreased monotonically. The relative minimum in the cross section for argon targets was independently found by Townsend and Bailey.[2] These measurements were not in agreement with classical predictions.

It was suggested that the observed phenomenon, known as the Ramsauer-Townsend effect, might be explained by means of a partial-wave analysis. This explanation was confirmed quantitatively by Holtsmark[3] who calculated the phase shifts for scattering of electrons by argon atoms. A condition for the Ramsauer-Townsend effect to occur is that the field of the atom be sufficiently strong so that for zero incident energy the phase shift of the zeroth-order partial wave is equal to $n\pi$, where n is a positive integer. As the incident energy is increased from zero, it is possible for this phase shift to first increase and then decrease back through the value $n\pi$. At this nonzero energy at which the phase shift equals $n\pi$, the zeroth-order partial cross section vanishes. If the other partial cross sections are negligible at this energy, a cross-section minimum may then occur. The appearance of a maximum in the cross section may be explained by somewhat similar considerations of the phase shifts and partial cross sections.

Thirty-one years after the discovery of the Ramsauer-Townsend effect in atoms, Barschall[4] and his collaborators measured total cross sections for neutrons scattered by a number of different heavy nuclei for the energy range 0.1 to 3 MeV. They observed that the cross section for a given target nucleus, instead of decreasing monotonically with energy as had been predicted theoretically, exhibited a broad minimum and a broad maximum. In addition, they noted that the position of the broad maximum for different nuclei appeared to shift to higher energies with increasing mass number. The theoretical confirmation of these low-energy-neutron total cross sections was obtained by Feshbach, Porter, and Weisskopf[5,6] with an optical model of the nucleus. Since 1952, the energy domain in which these broad maxima and minima have been observed has been extended to 100 MeV. These broad peaks have often been referred to as "neutron giant resonances," and as many as three such maxima have been observed for many heavy nuclei. The incident-neutron kinetic energies at which the maxima and minima are found are shown in Fig. 1 as a function of $A^{1/3}$, where A is the mass number of the target nucleus.[7]

It is our purpose to furnish, in the present analysis, a simple explanation of the observed phenomenon. We wish to describe the appearance of the broad maxima and minima in neutron cross sections within the frame-

* This work is supported in part through funds provided by the U. S. Atomic Energy Commission under contract AT(30-1)-2098.
† Present address: Lawrence Radiation Laboratory, Berkeley, California.
[1] C. Ramsauer, Ann. Physik **64**, 513 (1921); **66**, 546 (1921).
[2] J. S. Townsend and V. A. Bailey, Phil. Mag. **43**, 593 (1922); **44**, 1033 (1922).
[3] J. Holtsmark, Z. Physik **55**, 437 (1929).
[4] H. H. Barschall, Phys. Rev. **86**, 431 (1952); D. W. Miller, R. K. Adair, C. K. Bockelman, and S. E. Darden, *ibid.* **88**, 83 (1952).
[5] H. Feshbach, C. E. Porter, and V. F. Weisskopf, Phys. Rev. **96**, 448 (1954).
[6] C. Campbell, H. Feshbach, C. E. Porter, and V. F. Weisskopf, Massachusetts Institute of Technology Laboratory for Nuclear Science Technical Report 73, 1960 (unpublished).
[7] This plot is taken from Ref. 12.

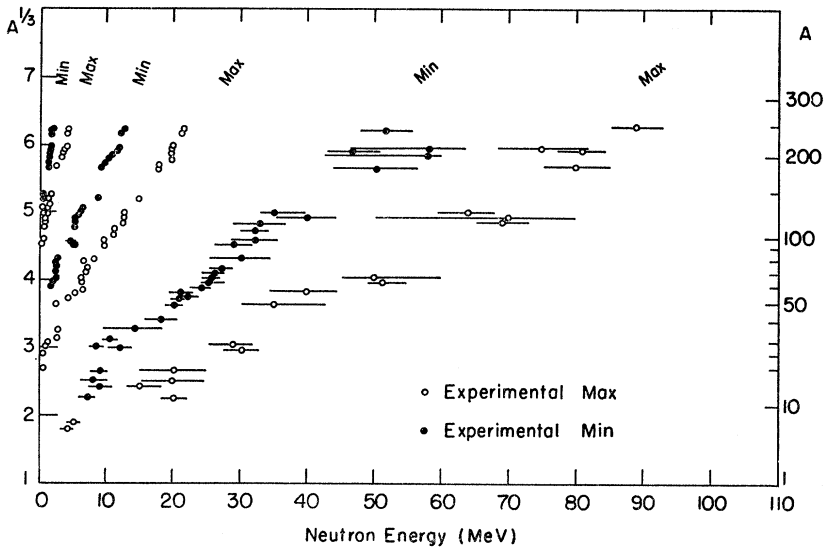

FIG. 1. Plot showing the measured positions in neutron energy and target mass number of the broad maxima and minima in neutron total cross sections.

work of the Glauber approximation and the optical model.[8] We have by no means attempted to construct a theory which will reproduce the measurements with accurate quantitative detail. Since the Glauber approximation is asymptotically correct for high-energy scattering, we will find it convenient to use a modification due to Riese.[9,10] This modification will enable us to calculate cross sections, by means of an optical potential, for incident neutron energies below 100 MeV with greater accuracy than is afforded by the usual high-energy approximation.

In Sec. II we briefly outline two earlier theoretical descriptions of neutron cross-section maxima. We begin the present analysis in Sec. III by investigating the neutron-nuclear total cross sections, within the framework of the Glauber approximation, and obtain the general conditions for the occurrence of maxima and minima. In the next section we very briefly consider scattering and absorption cross sections. In Sec. V we use the Glauber approximation, both with and without the modification of Riese, to express the cross sections in terms of an optical potential, and we illustrate the theory with some simple calculations. In Sec. VI we present some numerical results for the predicted energies of the cross-section maxima and minima, and give some quantitative comparisons of the energy dependence in the cross sections obtained from the approximations with that obtained from numerical calculations. We then briefly consider the energy dependence of the absorption and scattering cross sections separately. We conclude in Sec. VII with a short discussion of the roles played by the individual phase shifts in the appearance of cross-section maxima and minima.

[8] R. J. Glauber, *Lectures in Theoretical Physics* (Interscience Publishers, Inc., New York, 1959), Vol. I, p. 315.
[9] J. W. Riese, Ph.D. thesis, Massachusetts Institute of Technology, 1958 (unpublished).
[10] The existence of Ref. 9 was pointed out to the author by H. Feshbach (private communication).

II. SOME PREVIOUS ANALYSES

An early theoretical description of the appearance of neutron cross-section maxima and minima at high energies was given by Lawson.[11] The nucleus was represented by a uniform sphere with a potential well depth of approximately 30 MeV. A maximum in the cross section was assumed to occur when the average phase difference between that portion of the neutron wave which does traverse the nucleus and that which does not was equal to an odd multiple of π. A minimum was assumed to occur when this average phase difference was equal to an even multiple of π. The energies for the maxima corresponding to an average phase difference of π were estimated for several target nuclei and were consistent with experiment.

A more recent analysis of the neutron cross-section maxima and minima was given by Peterson[12] who referred to the phenomenon as a nuclear Ramsauer effect. In this analysis the nucleus was represented by a real square well of radius R. It was shown from geometry and Snell's law of refraction that the average chord length of a ray passing through a sphere of radius R is $\frac{4}{3}\alpha R$, where α depends upon the index of refraction of the sphere. In the high-energy limit, where the ratio of the potential strength V_0 to the incident energy E, approaches zero, α approaches unity. Let us denote the wave numbers of the neutron outside and inside the well by k and K, respectively. Then "the average phase difference Δ between the wave traversing the nucleus and that going around"[12] was given by Peterson as

$$\Delta=\tfrac{4}{3}\alpha(K-k)R. \tag{2.1}$$

The condition for a maximum in the cross section was then taken to be maximum destructive interference between the two wave components. This condition, in

[11] J. D. Lawson, Phil. Mag. 44, 102 (1953).
[12] J. M. Peterson, Phys. Rev. 125, 955 (1962).

turn, was assumed by Peterson to be equivalent to the condition that the average phase difference Δ be an odd multiple of π, i.e.,

$$\Delta = n\pi, \quad n = 1,3,5,\ldots, \text{odd}. \tag{2.2}$$

With n even, this expression was taken as the condition for a relative minimum in the cross section. We wish to question the validity of placing condition (2.2) on the average phase difference in order to secure a maximum in the cross section. Our reasons will be presented in the next section.

Other analyses have been given by Nemirovskii[13] who used a partial-wave expansion and a one-dimensional W.K.B. method, and by Mandl and Skyrme[13] who used a variational method. After the completion of the present analysis, a Letter by McVoy[14] appeared on this subject.

III. NEUTRON TOTAL CROSS SECTIONS

In this section we investigate neutron-nuclear total cross sections and describe the conditions under which, for a given nucleus, they may exhibit maxima and minima as the incident neutron energy is varied. The formalism we use is the Glauber diffraction approximation.[8] This approximation is asymptotically correct for high-energy scattering at small angles, and is not expected to be accurate for incident energies and target nuclei which together do not satisfy the condition $kR \gg 1$.

We begin the analysis by obtaining an approximate formula for the total cross section in terms of an integral, over impact parameters, of an expression involving a phase-shift function. This function of course depends in some manner upon the neutron-nuclear interaction but does not require the existence of an interaction potential. We then give the general conditions for the appearance of cross-section maxima and minima and show that the average value of the phase-shift function need not be an integral multiple of π at a cross-section maximum or minimum.

By virtue of the optical theorem, which relates the total cross section to the imaginary part of the forward elastic-scattering amplitude, an approximate expression for the total cross section is easily obtained. If the interaction between the incident nucleon and the target nucleus possesses azimuthal symmetry about the direction of the incident beam, then the elastic scattering amplitude, $f(\theta)$, may be expressed by means of the familiar partial-wave expansion,

$$f(\theta) = \frac{i}{2k} \sum_{l=0}^{\infty} (2l+1)(1-e^{2i\delta_l}) P_l(\cos\theta), \tag{3.1}$$

where δ_l is the phase shift of the lth partial wave, θ is the scattering angle, and $P_l(\cos\theta)$ is the lth Legendre polynomial. From the optical theorem the total cross section, σ, is given by

$$\begin{aligned} \sigma &= (4\pi/k)\,\mathrm{Im} f(0), \\ &= (2\pi/k^2) \sum_{l=0}^{\infty} (2l+1)(1-\mathrm{Re}e^{2i\delta_l}). \end{aligned} \tag{3.2}$$

For $kR \gg 1$, many partial waves may be expected to contribute to the cross section. If we let b denote the impact parameter of any particular segment of the wave front which sweeps over the region of interaction, the summation over the angular momenta l may be transformed to an integration over b by means of the Euler-Maclaurin summation formula. The total cross section may then be approximated by

$$\sigma = 2\int_0^{\infty} (1-\mathrm{Re}e^{i\chi(b)}) 2\pi b db, \tag{3.3}$$

where $\chi(b)$ is a phase-shift function which depends upon the interaction and is generally energy-dependent.

In the general case, where the interaction between the incident nucleon and the target nucleus does not possess azimuthal symmetry about the direction of the incident beam, the total cross section is given by[8,15]

$$\sigma = 2\int (1-\mathrm{Re}e^{i\chi(\mathbf{b})}) d^{(2)}\mathbf{b}, \tag{3.4}$$

where the phase-shift function now depends upon the impact-parameter vector $\mathbf{b}$ which lies in a plane perpendicular to the direction of the incident beam, and the integration is over this plane.

The general conditions for a relative maximum or minimum in the total cross section for a given nucleus are given by

$$\frac{\partial}{\partial E}\int \mathrm{Re}e^{i\chi(\mathbf{b})} d^{(2)}\mathbf{b} = 0 \tag{3.5}$$

and

$$\frac{\partial^2}{\partial E^2}\int \mathrm{Re}e^{i\chi(\mathbf{b})} d^{(2)}\mathbf{b} \neq 0. \tag{3.6}$$

In the present analysis we will be concerned primarily with condition (3.5). We must, however, always keep condition (3.6) in mind.

To demonstrate that the average phase difference need not be an integral multiple of π at cross-section maxima or minima, we begin be letting $\mathbf{r}$ be the position vector of the incident neutron with respect to the center of mass of the target nucleus. If the interaction vanishes identically for $|\mathbf{r}| > R$, then the phase-shift function $\chi(\mathbf{b})$ will be zero for impact parameters greater than R

[13] P. E. Nemirovskii, Zh. Eksperim. i Teor. Fiz. **30**, 551 (1956) [English transl.: Soviet Phys.—JETP **3**, 484 (1956)]; F. Mandl and T. H. R. Skyrme, Phil. Mag. **44**, 1028 (1953).

[14] K. W. McVoy, Phys. Letters **17**, 42 (1965).

[15] A derivation of the elastic-scattering amplitude for this general case is given in the high-energy approximation by V. Franco and R. J. Glauber (to be published).

and Eq. (3.4) becomes

$$\sigma=2\pi R^2\left(1-\frac{1}{\pi R^2}\int_{|\mathbf{b}|=0}^{R}\mathrm{Re}e^{i\chi(\mathbf{b})}d^{(2)}\mathbf{b}\right). \quad (3.7)$$

The negative of the second term in the bracket in Eq. (3.7) may be interpreted as the average value of the real part of $e^{i\chi(\mathbf{b})}$, which we shall denote by $\langle\mathrm{Re}e^{i\chi(\mathbf{b})}\rangle_{\mathrm{av}}$. The equation may then be written as

$$\sigma=2\pi R^2(1-\langle\mathrm{Re}e^{i\chi(\mathbf{b})}\rangle_{\mathrm{av}}). \quad (3.8)$$

In general, the phase-shift function $\chi(\mathbf{b})$ is complex.

Since particles are not being created, the imaginary part of the phase-shift function is non-negative. The absolute maximum value that the cross section may attain is then $4\pi R^2$ and occurs when the average of the real part of $-\exp[i\chi(\mathbf{b})]$ is unity. If we assume that $\chi(\mathbf{b})$ is a continuous function of the impact parameter for values of the impact parameter smaller than R, then the necessary and sufficient condition for the cross section to attain this absolute maximum is that the phase-shift function be an odd multiple of π for *all* $b<R$, so that

$$\chi(\mathbf{b})=n\pi, \quad \text{for} \quad b<R, \quad n=1,3,5,\ldots,\text{odd}. \quad (3.9)$$

This means that all portions of the wave traversing the nucleus interfere destructively with the incident beam. The condition (3.9) implies, of course, that the average of the phase-shift function, $\langle\chi(\mathbf{b})\rangle_{\mathrm{av}}$, must also be an odd multiple of π, i.e.,

$$\langle\chi(\mathbf{b})\rangle_{\mathrm{av}}=n\pi, \quad n=1,3,5,\ldots,\text{odd}. \quad (3.10)$$

Now this condition corresponds to Eq. (2.2) of the present paper or Eq. (2) of Ref. 12. However, $\chi(\mathbf{b})$ generally will not be independent of $\mathbf{b}$, and the average value of $-\mathrm{Re}\exp[i\chi(\mathbf{b})]$ will generally be less than unity.

In summary, then, the condition for a relative maximum in the cross section is a relative maximum in the average value of $-\mathrm{Re}\exp[i\chi(\mathbf{b})]$. This generally does not imply that the average value of $\chi(\mathbf{b})$ is an odd multiple of π. In general, it is incorrect to place condition (2.2) on the average value of the phase difference in order to secure a maximum in the cross section.

It is interesting to note from Fig. 1 that the measured energies at which the maxima and minima occur tend to increase with increasing mass number. It is therefore of interest to investigate theoretically how the energies at which the maxima and minima occur vary with nuclear size. If we assume that the phase-shift function depends in some unspecified manner upon the incident energy and the nuclear radius, the equation of the loci of maxima and minima in the E,R plane may be written as

$$\mathrm{Re}\frac{\partial}{\partial E}\int e^{i\chi(\mathbf{b},E,R)}d^{(2)}\mathbf{b}=0. \quad (3.11)$$

The slopes of these loci are then given by

$$\frac{dR}{dE}=\frac{(\partial^2/\partial E^2)\sigma(E,R)}{2\,\mathrm{Re}(\partial^2/\partial E\partial R)\int e^{i\chi(\mathbf{b},E,R)}d^{(2)}\mathbf{b}}, \quad (3.12)$$

where the expression on the right is to be evaluated at those values of R and E for which maxima or minima occur. At a relative maximum the numerator is negative, and at a relative minimum it is positive. Therefore the sign of the slope is basically determined by the sign of the denominator. An application of Eq. (3.12) will be illustrated in Sec. V.

IV. SCATTERING AND ABSORPTION CROSS SECTIONS

Thus far we have restricted ourselves to an analysis of only the neutron-nuclear total cross section. It is of interest to also consider the scattering cross section and the "absorption" cross section separately. The absorption cross section, σ_a, is given by the familiar expression

$$\sigma_a=\frac{\pi}{k^2}\sum_{l=0}^{\infty}(2l+1)(1-|e^{2i\delta_l}|^2), \quad (4.1)$$

where δ_l is the complex phase shift for the lth partial wave. In the Glauber approximation the absorption cross section is given by the analogous expression

$$\sigma_a=\int(1-|e^{i\chi(\mathbf{b})}|^2)d^{(2)}\mathbf{b}. \quad (4.2)$$

The scattering cross section σ_{sc} may be obtained by subtracting the absorption cross section, given by Eq. (4.2), from the total cross section, given by Eq. (3.4), and may be expressed in terms of the phase-shift function by

$$\sigma_{\mathrm{sc}}=\sigma-\sigma_a, \quad (4.3)$$

$$=\int|1-e^{i\chi(\mathbf{b})}|^2d^{(2)}\mathbf{b}. \quad (4.4)$$

V. CALCULATIONS WITH OPTICAL POTENTIALS

We now illustrate the theory developed in the preceding sections by considering optical models for the nucleus. We wish to emphasize that these models are extremely simple. Accurate agreement between the observed measurements and the predictions should not be expected. First of all, the approximations we have used may be inaccurate at the lower energies. In addition, the optical model is an incomplete description of the nucleus. Finally, the results will, of course, be sensitive to the shape and magnitude of the optical potential used. We have used only the simplest of shapes and we have not varied the magnitudes to obtain better fits.

We shall consider two approximate expressions for the relationship between the phase-shift function and

the optical potential. The first is a high-energy approximation, and is sufficiently accurate only if the magnitude of the potential is much smaller than the incident energy. Although this requirement is not satisfied very well for energies below 100 MeV, the approximation does give an indication that the general methods we have used are valid since the fit near 100 MeV is not unreasonable. We then consider a modification of the high-energy approximation which requires that the magnitude of the potential be only approximately smaller than the incident energy and consequently allows us to apply the results of Secs. III and IV to energies below 100 MeV.

Let us begin by writing the position vector $\mathbf{r}$ of a particular point on the wave front in terms of its impact parameter vector $\mathbf{b}$ and a vector $\mathbf{z}$ parallel to the direction of the incident beam so that $\mathbf{r}=\mathbf{b}+\mathbf{z}$. We then represent the scattering nucleus by an optical potential $V(\mathbf{r})$ which in general may be complex. If the magnitude of the potential is much smaller than the incident energy, then the phase-shift function is given in the high-energy approximation by[8]

$$\chi(\mathbf{b})=-\frac{1}{\hbar v}\int_{-\infty}^{\infty}V(\mathbf{b}+\mathbf{z})dz. \tag{5.1}$$

In this formula v is the relative velocity between the incident particle and the target nucleus. In obtaining Eq. (5.1) it is assumed that in passing through the region of interaction the nucleon is not deflected by the potential, and therefore this expression is a small-angle approximation.

We have used Eq. (5.1) with square-well potentials and have calculated the loci of the maxima and minima of the cross section σ in the $E,A^{1/3}$ plane. Anticipating the results presented in the next section, we find that these loci are in rough qualitative agreement with experiment for energies greater than approximately 50 MeV. We note also that the calculated maxima and minima all occur at energies below 110 MeV, as indeed do the measured maxima and minima. In Sec. VI we shall discuss in more detail the various optical potentials we have used in the calculations. Suffice it to note, for the present, that in the energy range considered, the optical potentials used are such that $|V|/E$ is not much smaller than unity. Consequently Eq. (5.1), which is based upon the assumption that $|V|/E\ll 1$, is not expected to be very accurate in the energy range of interest.

A modification of Eq. (5.1) has been made by Riese.[9] His result replaces the condition $|V|/E\ll 1$ by the less restrictive one $|V|/E\lesssim 1$. The condition $kR\gg 1$ is unchanged. For the case of a square-well potential, which was a case treated explicitly by Riese, the phase-shift function is now given by the expression

$$\chi(\mathbf{b})=\int_{-\infty}^{\infty}[K(\mathbf{b},z)-k]dz, \tag{5.2}$$

where

$$\begin{aligned}K(\mathbf{b},z)&=K, \quad r<R,\\ &=k, \quad r>R.\end{aligned}$$

This we recognize as the classical expression for the phase difference between that portion of a wave which traverses the sphere along an undeflected path and that which bypasses the sphere. It was obtained by explicitly taking into account the reflection of the incident wave at the first surface of the potential well. The same expression for the phase-shift function was obtained by Riese for a wide spectrum of potentials, ranging from the square-well potential to very slowly varying potentials.

In deriving Eq. (5.2), the reflection of the incident wave as it arrives at the nuclear surface is considered explicitly. All reflections of that portion of the wave which is refracted at the nuclear surface are neglected. The validity of this approximation will depend on having $|V|/E$ not too large, so that not many reflections occur, and on the small-angle approximation, so that those reflections which do occur do not contribute appreciably to the forward scattering. In addition, the actual refraction of the incident beam is neglected, i.e., the wave is assumed to traverse the region of interaction in an undeviated path along the direction of the incident beam, suffering only a position-dependent change of phase. As we have noted earlier, this approximation is valid if only small-angle scattering is treated.

Since we shall carry out our calculations for incident neutron kinetic energies as high as 100 MeV, where relativistic corrections tend to become significant, the wave number of the neutron in the potential well will be defined by means of the relativistic energy-momentum relation

$$(E+mc^2-V)^2=\hbar^2K^2c^2+m^2c^4, \tag{5.3}$$

where m is the mass of the incident particle. Then the phase-shift function $\chi(\mathbf{b})$ given by Eq. (5.2) may be expressed in terms of the optical potential $V(\mathbf{b},z)$ by

$$\chi(\mathbf{b})=k\int_{-\infty}^{\infty}\left\{\left[1-\frac{2V(\mathbf{b},z)}{\hbar kv}\left(1-\frac{1}{2}\frac{V(\mathbf{b},z)}{E+mc^2}\right)\right]^{1/2}-1\right\}dz. \tag{5.4}$$

By expanding the integrand we see that for $|V|/E\ll 1$ this expression reduces to Eq. (5.1).

Let us now examine some simple specific nuclear models. These models have been chosen, in part, to obtain manageable analytical expressions for the various cross sections which we calculate. Our use of them does not, of course, imply their accuracy or our endorsement of them as being realistic descriptions of the interactions.

We first consider a nucleus represented by a real square-well potential with range R and depth V_0, so that

$$\begin{aligned}V(\mathbf{r})&=-V_0, \quad r<R,\\ &=0, \quad r>R.\end{aligned} \tag{5.5}$$

In general, V_0 will be energy-dependent. It will be convenient to introduce the abbreviation

$$\beta=kR\left\{\left[1+\frac{2V_0}{\hbar kv}+\frac{V_0^2}{\hbar kv(E+mc^2)}\right]^{1/2}-1\right\}. \quad (5.6)$$

Then the phase-shift function, as expressed by Eq. (5.4), is given simply by

$$\begin{aligned}\chi(\mathbf{b})&=2\beta[1-(b/R)^2]^{1/2}, \quad b<R,\\ &=0, \quad b>R.\end{aligned} \quad (5.7)$$

It is interesting to note that the average phase-shift function is given by

$$\langle\chi(\mathbf{b})\rangle_{\text{av}}=\tfrac{4}{3}(K-k)R. \quad (5.8)$$

We recognize this to be simply the average phase difference Δ given by Eq. (2.1) when refraction is neglected, i.e., when α is unity. The cross section, as given by Eq. (3.8), may be written as

$$\sigma=\pi R^2(2+\beta^{-2}-\beta^{-2}\cos2\beta-2\beta^{-1}\sin2\beta). \quad (5.9)$$

In the high-energy limit as $|V|/E$ approaches zero, the total cross section becomes identical to that obtained by Glauber.[8]

A maximum or minimum in the cross section may occur when β satisfies

$$(1-2\beta^2)\cos2\beta+2\beta\sin2\beta=1. \quad (5.10)$$

The seven smallest positive solutions are given in Table I. The nth solution, β_n, approaches $\frac{1}{2}(n+\frac{1}{2})\pi$ for large n.

If we assume that the radius of the nucleus is given by

$$R=r_0A^{1/3}, \quad (5.11)$$

then the loci of maxima and minima in the $E,A^{1/3}$ plane are given by

$$A^{1/3}=\beta_nR/\beta r_0. \quad (5.12)$$

If we had used the high-energy approximation (5.1) for the phase-shift function, the loci would have been given by the simple expression

$$A^{1/3}=\beta_n\hbar v/r_0V_0(E). \quad (5.13)$$

Some numerical results obtained with Eqs. (5.12) and (5.13) are presented in the next section.

TABLE I. Positive solutions to Eq. (5.10) for β_n at cross section maxima and minima. The values of $\frac{1}{2}(n+\frac{1}{2})\pi$ are given for comparison. The values of $\sin2\beta_n$ are also shown.

n	β_n	$\frac{1}{2}(n+\frac{1}{2})\pi$	$\sin2\beta_n$
1	2.04	2.36	−0.81
2	3.81	3.93	0.97
3	5.40	5.50	−0.98
4	7.00	7.07	0.99
5	8.58	8.64	−0.99
6	10.16	10.21	0.99
7	11.74	11.78	−0.99
∞	$\frac{1}{2}(n+\frac{1}{2})\pi$	$\frac{1}{2}(n+\frac{1}{2})\pi$	$(-)^n$

If the optical potential is taken to be a complex square well, so that

$$\begin{aligned}V(\mathbf{r})&=-(V_0+iW_0), \quad r<R,\\ &=0, \quad r>R,\end{aligned} \quad (5.14)$$

where V_0 and W_0 are generally energy dependent, then the phase-shift function is complex and is given by Eq. (5.7), with V_0 in the Eq. (5.6) for β replaced by V_0+iW_0. If we let $\nu=\lambda+i\mu$, where λ and μ are given by

$$\begin{Bmatrix}\lambda\\ \mu\end{Bmatrix}=kR\begin{Bmatrix}\text{Re}\\ \text{Im}\end{Bmatrix}\left\{\left[1+\frac{2(V_0+iW_0)}{\hbar kv}+\frac{(V_0+iW_0)^2}{\hbar kv(E+mc^2)}\right]^{1/2}-1\right\}, \quad (5.15)$$

then the phase-shift function is given by Eq. (5.7) with β replaced by ν, and the total cross section may be written as

$$\sigma=\pi R^2\left\{2+\frac{\lambda^2-\mu^2}{(\lambda^2+\mu^2)^2}-\frac{e^{-2\mu}}{\lambda^2+\mu^2}\times\left[\frac{(\lambda^2-\mu^2)\cos2\lambda+2\lambda\mu\sin2\lambda}{\lambda^2+\mu^2}+2(\lambda\sin2\lambda-\mu\cos2\lambda)\right]\right\}. \quad (5.16)$$

Some numerical results for a complex square-well potential, showing the effect of the addition of an imaginary part to the potential on the positions of the maxima and minima, are given in the next section.

Since a complex optical potential gives rise to absorptive processes, we may now calculate the absorption cross section for a complex square-well potential. By means of Eqs. (4.2) and (5.7) we find

$$\sigma_a=\pi R^2[1+\tfrac{1}{2}\mu^{-1}e^{-4\mu}-\tfrac{1}{8}\mu^{-2}(1-e^{-4\mu})]. \quad (5.17)$$

The scattering cross section may then be obtained from Eqs. (4.3), (5.16), and (5.17).

The expression (5.16) indicates that the total cross section tends to be an oscillatory function of the incident energy. On the other hand, Eq. (5.17) indicates that the absorption cross section tends to be a rather slowly varying function which possesses maxima and minima only if μ possesses maxima and minima. Therefore the scattering cross section, which is the difference between σ and σ_a, also tends to be an oscillatory function of the energy with maxima and minima at energies close to those of the corresponding maxima and minima in the total cross section. To illustrate this explicitly we shall present some numerical results for these cross sections in the next section.

We have noted, in Sec. III, that the measured energies at which the cross-section maxima and minima occur tend to increase with increasing target mass

number. We have obtained an expression, given by Eq. (3.12), for the slopes of the loci of the maxima and minima in the E,R plane. To obtain some simple theoretical implications of the observed relation $dR/dE>0$, we shall apply Eq. (3.12) to the case of a real square well whose depth may be energy-dependent. Using the phase-shift function for a square well given by Eq. (5.7), we find that the sign of the denominator on the right-hand side of Eq. (3.12) is that of

$$(\partial^2/\partial E\partial R)[R^2\beta^{-2}(\cos 2\beta+2\beta\sin 2\beta-1)]. \quad (5.18)$$

If we consider the high-energy limit, then β becomes $V_0R/\hbar v$ and the sign of the expression (5.18) reduces to that of

$$-\sin 2\beta(d/dE)(|V_0|/v), \quad (5.19)$$

where this expression is to be evaluated at those values of R and E corresponding to maxima and minima in the total cross section. At cross-section maxima, $\sin 2\beta$ is always negative (see Table I), and at cross-section minima it is always positive. Thus the signs of the slopes dR/dE are opposite to those of $d(|V_0|/v)/dE$. If we require positive values for dR/dE, as the experiments tend to suggest we should, then we must have

$$(d/dE)(|V_0|/v)<0. \quad (5.20)$$

This condition is always satisfied, for example, by a potential well whose strength $|V_0|$ remains constant or decreases with increasing incident energy.

If we consider the modified high-energy approximation, Eq. (5.4), then β is given by Eq. (5.6). Some algebra shows that the condition $dR/dE>0$ then implies

$$\left(1+\frac{V_0}{E+mc^2}\right)\left(1+\frac{dV_0}{dE}\right)<\left[1+\frac{2V_0}{\hbar kv}+\frac{V_0^2}{\hbar kv(E+mc^2)}\right]^{1/2}. \quad (5.21)$$

If the square well is attractive, i.e., $V_0>0$, then the inequality (5.21) is satisfied, for example, if $dV_0/dE\leq 0$.

VI. NUMERICAL RESULTS AND DISCUSSION

In this section we present some numerical results of the calculations for the loci of cross-section maxima and minima in the $E,A^{1/3}$ plane. We also compare total cross sections obtained from the approximations we have used with those calculated from numerical solutions of the Schrödinger equation. We conclude by briefly discussing the energy dependence of the scattering and absorption cross sections.

For the calculations presented in this section we have taken the depths of the various potential wells to be energy-dependent. Their dependence upon the energy is represented by simple assumed analytical forms which approximate the energy variation of the well depths obtained by Bowen *et al.*[16] The assumed forms for the real and imaginary parts of the potential well depths are plotted as solid curves in Fig. 2. Since it is not our aim to calculate optical potentials, we have not attempted to vary the potential depths to yield better fits to the cross-section measurements. In Fig. 2 we also show the corresponding energy dependence obtained by Bowen *et al.* For both the real and imaginary parts of the potential, they use the Woods-Saxon radial dependence

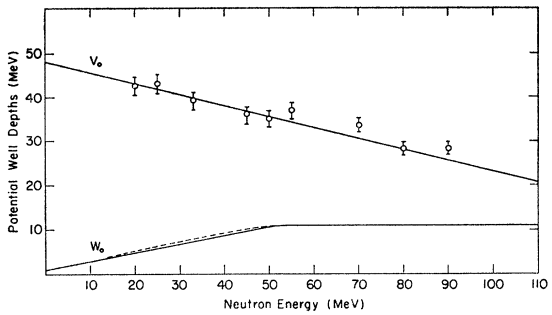

FIG. 2. The depths used for the real and imaginary parts of the potential wells as a function of neutron energy. The values obtained by Bowen *et al.* (Ref. 16) for the real part V_0 are shown as points with $\pm 5\%$ error bars. The broken curve is the imaginary part W_0 used by Bowen *et al.*, and was obtained from neutron absorption cross sections. The solid curves represent assumed analytical forms for the well depths used in the present calculations. For energies greater than 55 MeV the broken and solid curves are identical.

$$\rho(r)=(1+e^{(r-R)/a})^{-1}, \quad (6.1)$$

with $R=1.25A^{1/3}$ F and $a=0.6$ F. Relativistic corrections would decrease the magnitudes of their well depths by a few percent at higher energies. We have estimated this effect by taking the magnitude of the real part of the assumed analytical potential to be slightly smaller at higher energies than the magnitude which they have given.

The loci of cross-section maxima and minima in the $E,A^{1/3}$ plane, calculated from the usual high-energy approximation, Eq. (5.1), are shown in Fig. 3 for a square-well optical potential. We have taken $R=1.25A^{1/3}$ F. In Fig. 4 we show the loci curves obtained when the phase-shift function is calculated from the modified high-energy approximation, Eq. (5.4).

A comparison of Figs. 3 and 4 shows that the modified high-energy approximation improves the results both quantitatively and qualitatively. If we had shown the calculated loci for all n, then Fig. 3, in which the usual high-energy approximation is used, would have exhibited an infinite number of maxima and minima in the total cross section for any given nucleus. On the other hand, Fig. 4, in which the modification is used, would have shown that the cross section for any given nucleus has only a finite number of maxima and minima. To see this more explicitly, let us define a wave number at zero energy, K_0, to be

$$K_0=[2m\hbar^{-2}V_0(0)]^{1/2}, \quad (6.2)$$

[16] P. H. Bowen, J. P. Scanlon, G. H. Stafford, J. J. Thresher, and P. E. Hodgson, Nucl. Phys. 22, 640 (1961).

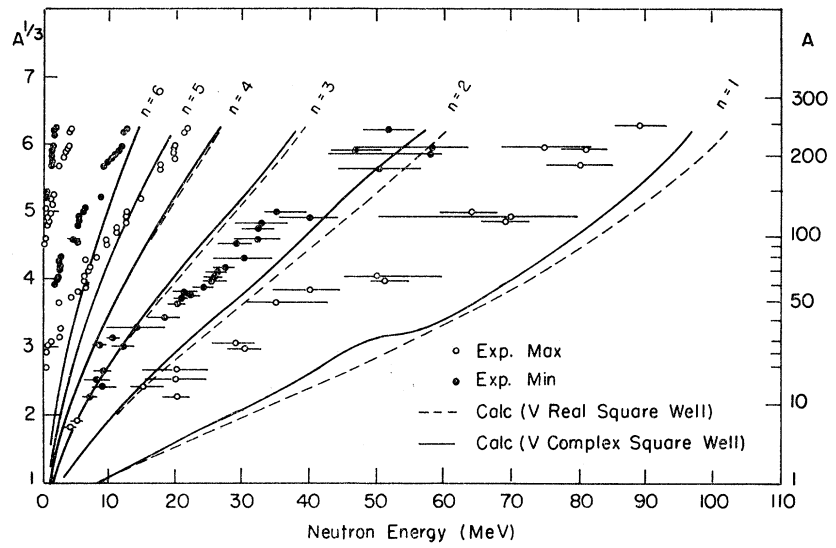

FIG. 3. Plot showing the calculated loci of maxima and minima (curves), together with the observed values (points) taken from Fig. 1. The phase-shift function is given by the high-energy approximation Eq. (5.1). The broken curves are obtained by using a real square-well potential, and the solid curves by using a complex square-well potential. The well depths used are shown in Fig. 2.

and set n equal to 7 in Eq. (5.12). Then the modified high-energy approximation with a square-well potential predicts that for A smaller than

$$\beta_7^3\{K_0^2r_0^2[1+V_0(0)/2mc^2]\}^{-3/2}$$

there are no more than three broad maxima and three broad minima in the total cross section. The value of β_7, shown in Table I, is 11.74. In our calculations we have used $r_0=1.25$ F and $V_0(0)=48$ MeV. With these values, Eq. (5.12) yields the result that for $A<225$ there are no more than three maxima and three minima in the total cross sections. This is in agreement with observation.

It is worth noting that the agreement of the calculations with the measurements for neutron energies greater than approximately 40 MeV is considerably improved by taking the imaginary part of the potential

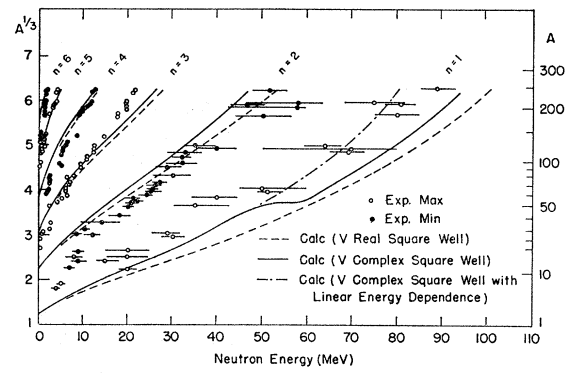

FIG. 4. Plot showing the calculated loci of maxima and minima (curves), together with the observed values (points) taken from Fig. 1. The phase-shift function is given by the modified high-energy approximation, Eq. (5.4). The broken curves are obtained by using a real square-well potential, and the solid curves by using a complex square-well potential. The well depths are shown in Fig. 2. The dot-dashed curve for the $n=1$ locus is calculated with W_0 given in Fig. 2 for $E<40$ MeV and with the linear extrapolation of that segment of the curve for energies greater than 40 MeV.

for energies greater than 40 MeV to be greater in magnitude than that shown in Fig. 2. Thus if we represent W_0 by the solid curve shown in Fig. 2, for energies less than 40 MeV, over which range it is linear, and extrapolate it linearly, for example, to higher energies, then the $n=1$ locus would be given by the dot-dashed curve in Fig. 4. The effect of this change in W_0 upon the $n=2$ locus is negligibly small. This is to be expected since for $A\lesssim 250$ this locus does not go above $E\approx 45$ MeV. There is, of course, no effect at all upon the other loci if the calculations are restricted to $A\lesssim 250$.

The agreement of the calculations with the measurements for energies greater than approximately 40 MeV can be improved still further by choosing the energy dependence of W_0 to lie somewhere between that shown in Fig. 2 and the linear extrapolation described above.

The small shoulder which appears in both Figs. 3 and 4 near 50 MeV in the $n=1$ loci calculated from the complex square-well potential of Fig. 2, arises from the rapid decrease in the slope of the imaginary part, W_0, in this energy region.

By comparing the solid curves with the corresponding broken curves in both Figs. 3 and 4, we see that the introduction of a small imaginary part to the potential does not alter the positions of the maxima and minima appreciably. This may perhaps be interpreted to indicate that as long as absorption is not very predominant, then the absorption processes do not play a significant role in determining the positions of these broad maxima and minima, and maxima and minima similar to those which appear in the total cross section also reveal themselves in the scattering cross sections. We shall explicitly demonstrate this with some numerical calculations later in this section.

For low energies and large values of n, e.g., $n\gtrsim 3$, the results for the loci curves obtained by using the modified high-energy approximation, Eq. (5.4), with a square-well potential, are close to those obtained in Ref. 12.

This similarity in the results may be explained by first noting that in the limit of zero energy, α is $\frac{3}{2}$ and condition (2.2) becomes

$$K_0R=\tfrac{1}{2}n\pi. \tag{6.3}$$

This equation determines the $A^{1/3}$ intercepts obtained in Ref. 12. On the other hand, the results obtained from the modification, Eq. (5.4), with a real square-well potential is, in the limit of zero energy,

$$K_0R=\beta_n[1+V_0(0)/2mc^2]^{1/2}, \tag{6.4}$$

where the values for β_n are given in Table I. The ratio of the value for K_0r_0 used in the present paper to that used by Peterson is 1.065. The ratios of the values obtained in Ref. 12 for the $A^{1/3}$ intercepts to the corresponding values obtained in this paper are given in Table II. These ratios approached 1.08 as n approaches

TABLE II. Ratios of $A^{1/3}$ intercepts in the loci curves calculated from the Peterson condition, Eq. (2.2), for a real square well with $V_0(0)r_0^2$ equal to 66 MeV F², to $A^{1/3}$ intercepts calculated from the modified high-energy approximation, Eq. (5.4), for a real square well with $V_0(0)r_0^2$ equal to 75 MeV F².

Locus number (n)	Ratio of $A^{1/3}$ intercepts
1	0.83
2	0.89
3	0.94
4	0.97
5	0.99
6	1.00
∞	1.08

infinity. We note that for $n=6$ the difference between the two calculated $A^{1/3}$ intercepts turns out to be smaller than 0.5% for the values of the various parameters which were used. If the values which were chosen

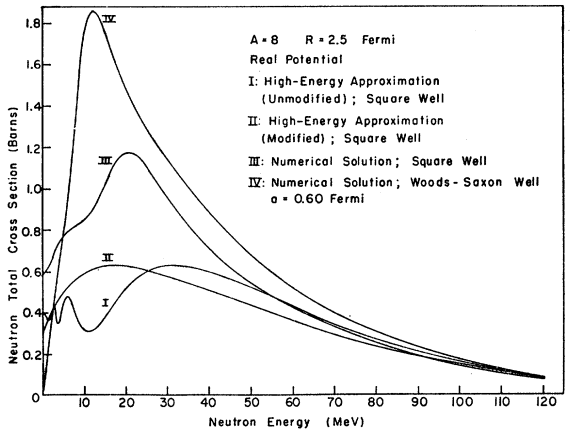

FIG. 5. Calculated neutron total cross sections as a function of neutron energy for real square-well and Woods-Saxon potentials for target mass number 8. The radius of the wells is taken to be 2.5 F. Curves I and II are obtained from the high-energy approximation with Eq. (5.1) and the modification (5.4), respectively, with a square well. Curves III and IV are numerical solutions of the Schrödinger equation with a square well and a Woods-Saxon well, respectively. The depths of the potentials are given in Fig. 2.

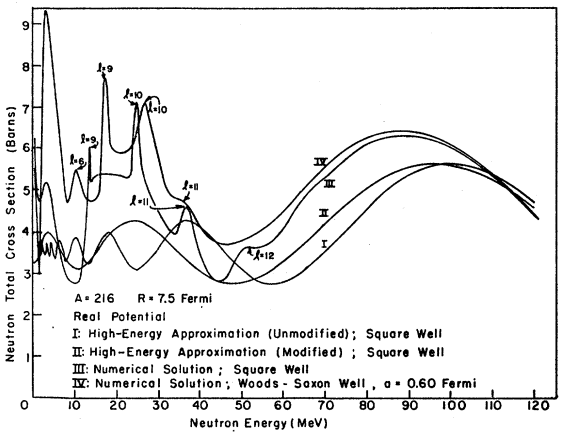

FIG. 6. Calculated neutron total cross sections as a function of neutron energy for real square-well and Woods-Saxon potentials for target mass number 216. The radius of the well is taken to be 7.5 F. Curves I and II are obtained from the high-energy approximation with Eq. (5.1) and the modification (5.4), respectively, with a square well. Curves III and IV are numerical solutions of the Schrödinger equation with a square well and a Woods-Saxon well, respectively. The depths of the potentials are given in Fig. 2. The orbital angular momenta l corresponding to the resonant partial waves are indicated.

for K_0r_0 had been the same in both papers, there would have been an even larger discrepancy in the $A^{1/3}$ intercepts for $n\leq 6$.

In the limit of infinite neutron kinetic energy, the discrepancy in $A^{1/3}$ between the two theories varies from 50% for infinite values of n, to 39% for $n=6$, to 15% for $n=1$.

It is interesting to compare the total cross sections obtained from the approximations we have used with those calculated numerically from the Schrödinger equation. For such comparisons we shall consider the cases $A=8$ and $A=216$, with $R=1.25A^{1/3}$ F. The energy dependence of the well depths, V_0 and W_0, which we shall use is again given in Fig. 2. The numerical solutions of the Schrödinger equation were very kindly furnished by E. H. Auerbach. In Figs. 5 and 6 we show the total cross sections for a real potential, as a function of neutron energy. We have taken the value of a in Eq. (6.1) to be 0.60 fermi.

For the nucleus $A=8$, curves I and II in Fig. 5 indicate that in the high-energy region the total cross section obtained from the usual high-energy approximation is similar to that obtained with the modification. This, of course, is not surprising since the two cross sections are expected to differ appreciably only when the magnitude of the potential is not much smaller than the incident energy. At lower energies, however, we note that the cross section obtained with the modification exhibits only one broad maximum, whereas the cross section obtained without the modification exhibits an infinite number of maxima. For clarity, we have drawn only the last three maxima in curve I. In addition, the high-energy maximum occurs at rather different positions in these two curves.

The finite number of maxima and minima in curves obtained from the modified high-energy approximation can be understood by recalling the definition of β given in Eq. (5.6) and noting that curve I is obtained by using the high-energy limit of that equation, $\beta \sim V_0 R/\hbar v$. Therefore curve I may be transformed into curve II by having it "stretched" to the left from the ordinate axis, $E=0$, while keeping the ordinates of the curve the same. The infinite number of maxima and minima at low energies in curve I are thereby eliminated since they are "stretched" out of the physical region, $E \geq 0$.

Let us next consider the two numerical solutions. The quantitative agreement between the cross section obtained from the numerical solution to the Schrödinger equation with the square-well potential, shown in curve III of Fig. 5, and the approximate cross sections, shown in curves I and II, is good at high energies. Below 50 MeV the quantitative agreement becomes poor. This, of course, is not surprising since for energies below 50 MeV, kR becomes smaller than 4 and $|V|/E$ becomes greater than 0.7. Thus the restrictions for curve II, namely that kR be much greater than unity and $|V|/E$ be approximately smaller than unity, tend to be violated below 50 MeV. Nevertheless we note that the qualitative agreement between the approximate cross section given in curve II and the cross section obtained numerically and shown in curve III, is not bad. The positions of the maxima in these cross sections are within a few MeV of each other.

The cross section obtained from the numerical solution to the Schrödinger equation with a Woods-Saxon potential, shown in curve IV, agrees quantitatively with the other cross sections in Fig. 5 in the high-energy region. Although the magnitude of this cross section at lower energies is considerably larger than those of the other cross sections shown in this figure, the qualitative features are similar in many respects to those of curves II and III.

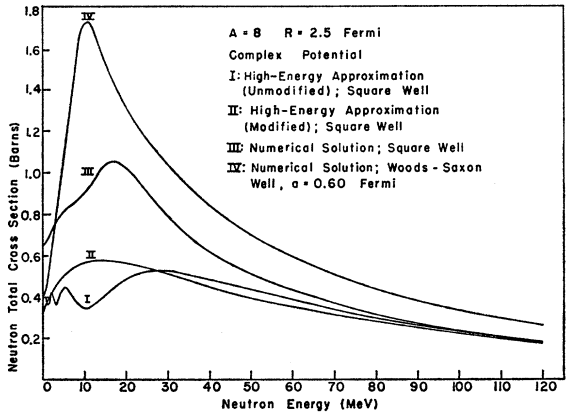

FIG. 7. Calculated neutron total cross sections as a function of neutron energy for complex square-well and Woods-Saxon potentials for target mass number 8. The radius of the well is taken to be 2.5 F. Curves I and II are obtained from the high-energy approximation with Eq. (5.1) and the modification (5.4), respectively, with a square well. Curves III and IV are numerical solutions of the Schrödinger equation with a square well and a Woods-Saxon well, respectively. The depths of the potentials are given in Fig. 2.

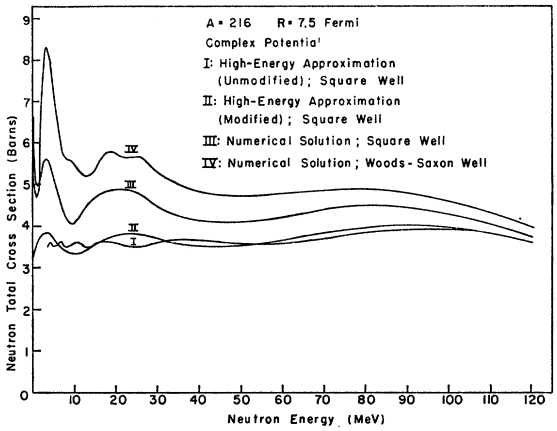

FIG. 8. Calculated neutron total cross sections as a function of neutron energy for complex square-well and Woods-Saxon potentials for target mass number 216. The radius of the well is taken to be 7.5 F. Curves I and II are obtained from the high-energy approximation with Eq. (5.1) and the modification (5.4), respectively, with a square well. Curves III and IV are numerical solutions of the Schrödinger equation with a square well and a Woods-Saxon well, respectively. The depths of the potentials are given in Fig. 2.

In comparing the approximate cross sections for the $A=216$ target, shown by curves I and II in Fig. 6, comments similar to those regarding the corresponding cross sections for the $A=8$ target may be made. The numerical solution for the cross section for a square-well potential, shown in curve III, exhibits relatively narrow resonances near 14, 25, and 37 MeV, and a shoulder near 52 MeV. If we were to average this cross section over energy intervals of say several MeV, the effects of these resonances would be eliminated or would show up rather weakly and we would find curve II to be in reasonable qualitative agreement with curve III. Similarly, if in the numerical solution for the Woods-Saxon well, shown in curve IV, we were to average the cross section over energy intervals of several MeV, then the shoulder near 36 MeV and the resonances near 11, 17, and 27 MeV would be eliminated or would show up rather weakly. We would then find curve II to be in reasonable qualitative agreement with curve IV.

In Figs. 7 and 8 we show the total cross-section curves for the case in which the well depths of the various optical potentials are now taken to be complex functions. These figures indicate that the addition of an absorptive part to the potential tends to flatten the curves. In addition there is no longer a relatively simple relationship between the two approximate cross sections obtained with and without the modification (5.4), i.e., between curves I and II. To transform curve I into curve II, we must now not only stretch it from the left, $E=0$, but we must also elevate its mountains and depress its valleys. Another effect of adding an absorptive part to the potential is to shift the positions of the

cross-section maxima and minima to slightly lower energies. A comparison of curves III and IV in Fig. 6 with the corresponding curves in Fig. 8 shows that the addition of an absorptive part to the potential completely eliminates or greatly weakens the relatively sharp resonances that appear with a real potential.

A comparison of Figs. 5 and 7 indicates that for small nuclei the addition of a small absorptive part to the optical potential does not affect the total cross sections greatly. On the other hand, a comparison of Figs. 6 and 8 indicates that for large nuclei the addition of a small absorptive part to the potential makes an appreciable difference in the cross section. We note that in addition to virtually eliminating the effects of all the narrow resonances in curves III and IV, the insertion of an absorptive part to the potential has tended to make curves II, III, and IV more qualitatively similar, even at low energies. For example, in Fig. 8 the positions of the maxima and minima obtained from the modified high-energy approximation are 91.5, 44, 23.5, 11, 4, and 1 MeV. The corresponding positions obtained from the numerical solution are 83, 44, 21, 10, 3.5, and 1.5 MeV. Although the positions of the high-energy maximum in the two calculations differ by 8.5 MeV, or 10%, we see that the maximum is extremely broad and that the cross section varies very slowly at these high energies. Thus in curve II the cross section at 83 MeV (which is 8.5 MeV below the high-energy maximum in this curve) differs from the cross section at the maximum (i.e., at 91.5 MeV) by less than one percent. In addition, the Schrödinger equation which is used to obtain curve III does not include any relativistic corrections.

As we have noted in Secs. IV and V, the high-energy approximation may be used to analyze the absorption and scattering cross sections separately. The approximate expressions for these cross sections for a complex square-well potential have been derived in Sec. V and are given by Eqs. (5.17), (5.16), and (4.3). In the present calculations we shall confine ourselves to a target nucleus with mass number 216. In Figs. 9 and 10 we show the total, absorption, and scattering cross sections obtained from complex potentials. The points in Fig. 10 are measured values[16,17] of the total cross sections of neutrons on lead.

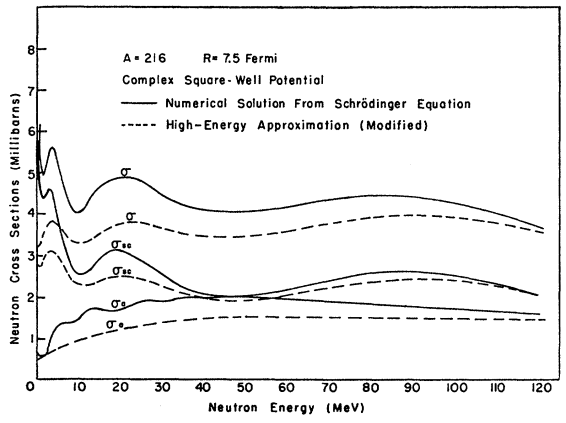

FIG. 9. Calculated neutron total, scattering, and absorption cross sections as a function of neutron energy for a complex square-well potential for target mass number 216. The depths of the potential are given in Fig. 2. The radius of the well is taken to be 7.5 F. The solid curves are numerical solutions for the cross sections obtained from the Schrödinger equation. The broken curves are obtained from the modified high-energy approximation, Eq. (5.4).

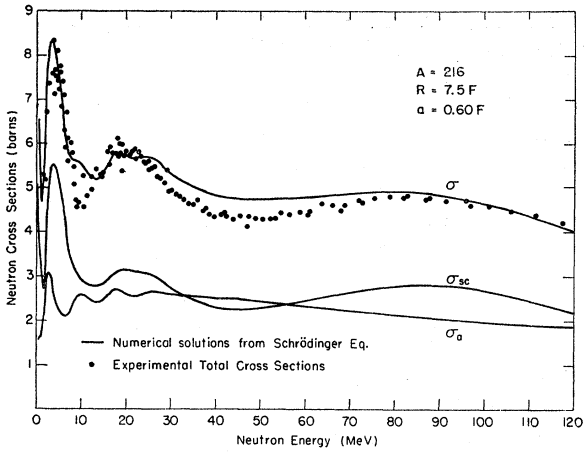

FIG. 10. Neutron total, scattering, and absorption cross sections as a function of neutron energy, numerically calculated from the Schrödinger equation with a complex Woods-Saxon well for target mass number 216. The depths of the potentials are given in Fig. 2. The radius of the well is taken to be 7.5 F. The measured total cross sections are shown as points.

From these figures we note that the main qualitative features of the total cross-section curves obtained from the numerical solutions of the Schrödinger equation are reproduced fairly well by those of the corresponding scattering-cross-section curves, particularly at high energies where the absorption cross section is a very slowly varying function of the energy. At lower energies, the oscillation in the absorption cross sections obtained from the numerical solutions, which arise from the small volume-absorption potential used, have an appreciable effect on the qualitative features of the total cross sections. For the Woods-Saxon well, for example, the shallow minimum in the total cross section shown near 22 MeV, shown in Fig. 10, corresponds in part to the relative minimum in the absorption cross section in that energy region.

Since at high energies the absorption cross section is a rather slowly varying function of the energy, we may attribute at least the first (high-energy) maximum and minimum in the total cross section solely to the first (high-energy) maximum and minimum in the scattering cross section. The absorption processes at these energies only serve to shift the position of the maximum and minimum by a small amount.

[17] *Neutron Cross Sections,* compiled by D. J. Hughes and R. Schwartz, Brookhaven National Laboratory Report BNL-325 (Superintendent of Documents, U. S. Government Printing Office, Washington, D. C., 1958), 2nd ed.

From Fig. 9 we note that the total, absorption, and scattering cross sections obtained from the modified high-energy approximation exhibit roughly the same qualitative features as those obtained from the numerical solutions, except in the absorption cross section at low energies where the numerical solution exhibits some oscillations. We note that in this approximation, the main features of the total-cross-section curve are reproduced quite well by the scattering-cross-section curve.

VII. PARTIAL-WAVE ANALYSES

We have made no attempt to investigate the cross-section maxima and minima by means of a detailed optical-model analysis of the phase shifts. Although it is certain that potentials different from those we have considered would fit the measurements more accurately, we have not attempted to compute them. However, in order to obtain some understanding of the roles played by the individual phase shifts, we shall consider some special cases and illustrate what occurs in these examples. We shall restrict our analysis to incident neutron energies greater than 0.5 MeV.

Suppose we consider a heavy nucleus, $A=216$. If the optical potential is either a real square well or a real Woods-Saxon well, whose depths are given in Fig. 2, then the corresponding total cross sections are given by curves III and IV in Fig. 6. A partial-wave analysis shows a number of resonances present in these cross sections. The values of the orbital angular momenta l corresponding to the resonant partial waves are indicated on the curve. Reference to Fig. 6 reveals that the three broad peaks are not caused by these resonances. This may be seen more easily if we consider the effect of adding a small imaginary part to the potential. The total cross sections are then given by curves III and IV in Fig. 8. The addition of a small absorptive part to the square-well potential is seen to eliminate the effects of all the resonances that previously appeared so strongly. Nevertheless, the three broad maxima still remain. The addition of an absorptive part to the Woods-Saxon potential almost completely eliminates the effects of the resonances that appeared previously. This is also clearly indicated by the scattering cross section given in Fig. 10. The three broad maxima, however, still remain in the total and scattering cross sections.

Let us now examine the partial cross sections for this case. In Table III we show the energies $E_{\max}$ at which the total cross section attains its maxima together with the values of these maxima.[18] We also show the ratios of the significant partial cross sections to the total cross section at the energies $E_{\max}$. We see that no one partial cross section is much greater than all the others and that at a cross-section maximum there are many partial cross sections which contribute appreciably.

The broad cross-section maxima which we have considered are not caused by a resonance due to any single phase shift, but rather by a joint effort on the part of many phase shifts to pool their resources and contribute a large share to the total cross section. This, no doubt, may often occur in the energy region where one or more partial cross sections happen to attain their maximum values.

TABLE III. Ratio of significant partial cross sections to the total cross section at energies for which the total cross section attains a relative maximum. The results are shown for a complex Woods-Saxon well (CWSW) and a complex square well (CSQW) for a nucleus with mass number 216. The corresponding values of the maximum cross sections and their energy positions are also given.

Potential	CWSW	CSQW	CWSW	CSQW	CWSW	CSQW
$\sigma_{\max}$ (barns)	4.9	4.5	≈5.7	4.9	8.3	5.6
$E_{\max}$ (MeV)	79	83	≈21	21	3.5	3.5
l	Ratio of partial cross section, $\sigma^{(l)}(E_{\max})$, to total cross section, $\sigma_{\max}$.					
0	0.003	0.004	0.010	0.015	0.020	0.017
1	0.010	0.011	0.028	0.026	0.140	0.371
2	0.017	0.018	0.054	0.088	0.339	0.467
3	0.023	0.026	0.083	0.083	0.396	0.088
4	0.031	0.031	0.119	0.139	0.024	0.015
5	0.038	0.045	0.170	0.236	0.080	0.042
6	0.046	0.048	0.199	0.240		
7	0.054	0.058	0.146	0.089		
8	0.065	0.076	0.068	0.035		
9	0.075	0.077	0.098	0.031		
10	0.087	0.084	0.024	0.015		
11	0.100	0.109				
12	0.111	0.128				
13	0.114	0.126				
14	0.101	0.100				
15	0.068	0.045				
16	0.033	0.010				
17	0.014	0.002				

ACKNOWLEDGMENTS

The author would like to thank Professor Herman Feshbach for referring him to the thesis of Riese and for a critical reading of the manuscript. He is indebted to Dr. Elliot H. Auerbach for the numerical solutions of the Schrödinger equation. Thanks are due to Mrs. Mida Aitken for assistance in programming.

[18] For the second broad maximum of curve IV in Fig. 8, since the cross-section curve in that region is perturbed by the oscillations in the absorption cross section we have chosen the position of the maximum to be at approximately 21 MeV, i.e., at approximately the position of the scattering cross-section maximum.